EPR in Protein Science

Intrinsically Disordered Proteins

Malte Drescher

Abstract Intrinsically disordered proteins (IDPs) form a unique protein category characterized by the absence of a well-defined structure and by remarkable conformational flexibility. Electron Paramagnetic Resonance (EPR) spectroscopy combined with site-directed spin labeling (SDSL) is amongst the most suitable methods to unravel their structure and dynamics. This review summarizes the tremendous methodological developments in the area of SDSL EPR and its applications in protein research. Recent results on the intrinsically disordered Parkinson's disease protein α-synuclein illustrate that the method has gained increasing attention in IDP research. SDSL EPR has now reached a level where broad application in this rapidly advancing field is feasible.

Keywords α-Synuclein · DEER/PELDOR · EPR · Intrinsically disordered proteins · Site-directed spin labeling

Contents

M. Drescher
Department of Chemistry, Zukunftskolleg, and Konstanz Research School Chemical Biology, University of Konstanz, 78457 Konstanz, Germany
e-mail: malte.drescher@uni-konstanz.de

The main purpose of this chapter is to summarize the state of the art in Electron Paramagnetic Resonance (EPR) spectroscopy combined with spin-labeling approaches as a tool for studying structure and dynamics of proteins. It should give the non-specialist reader an overview of the tremendous methodological developments and applications which have a huge impact on the field of biophysics, biology, and biochemistry. In particular, contributions of site-directed spin labeling EPR (SDSL EPR) to the rapidly advancing field of Intrinsically Disordered Proteins (IDPs) are described.

SDSL EPR as pioneered by W. L. Hubbel and co-workers has become a powerful tool for studying structure and dynamics of macromolecules, in particular biological macromolecules as proteins, which do not necessarily contain endogenous paramagnetic centers [1–4]. While SDSL EPR is applied to many bio-macromolecules, this chapter provides a rather selective insight into the field of SDSL EPR of proteins and is organized as follows.

First a basic introduction into approaches of SDSL of proteins is given, followed by a summary of the important approaches for mobility measurements, accessibility studies, and distance determination. Finally, we will address IDPs. Since structure and dynamics of IDPs drastically depend on the environment and corresponding details are notoriously difficult to unravel by NMR or X-ray structure determination, SDSL EPR can significantly contribute in the investigation of those systems. To showcase the use of SDSL EPR in this field, recent results on α-synuclein being a canonical model among the IDPs are reviewed.

1 Site-Directed Spin-Labeling of Proteins

Usually, nitroxides are used as spin-labels in SDSL EPR [5, 6]. However, with increasing spread of high-field EPR the relevance of other paramagnetic labels, e.g., Gd^{3+}, could gain increased relevance [7, 8]. Nitroxides are stable free radicals of the general form $\cdot O-NR^1R^2$. The unpaired electron required for EPR detection is (de-) localized on the N–O bond, about 40% of the spin density at the nitrogen atom and 60% at the oxygen atom. Since many biological macromolecules are diamagnetic, the nitroxide resonance is most often the only signal in the EPR spectrum. Nitroxide radicals are very stable, e.g., they can be stored for months under ordinary conditions. This stability is mainly due to steric protection of the N–O bond. Other parts of the molecule can be modified in order to attach the radical covalently to larger molecules [9].

Nitroxides can be used either as spin probes or as spin labels. Spin probes are subject to non-covalent interactions with the system under study. In many cases, spin probes very similar to one component of the system, e.g., spin-labeled lipids, are introduced. In contrast, spin labels are covalently linked to a complex structure, in many cases to a specific site, e.g., of a protein (SDSL) [10]. An alternative approach includes spin labeling of ligands interacting with the protein under study [11, 12].

The most common spin labeling strategy for proteins uses cysteine substitution mutagenesis followed by modification of the unique sulfhydryl group with specific

Fig. 1 *Left*: Structure of MTSSL bound to a cysteine residue within an amino acid sequence (*shaded*). The rotational degree of freedom caused by participating single bonds is indicated. *Right*: The unnatural spin-labeled amino acid TOAC
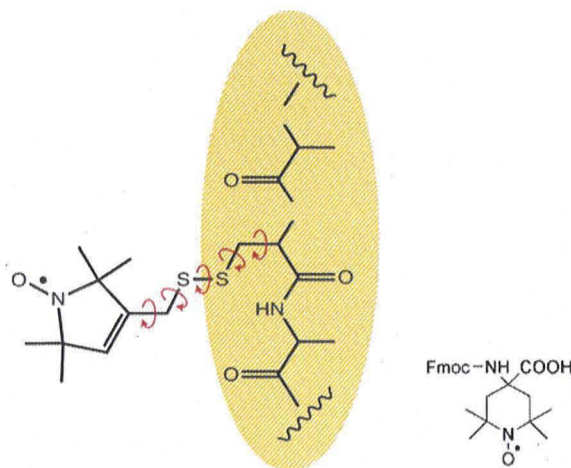
labeling agents, e.g., MTSSL (1-oxyl-2,2,5,5-tetra-methylpyrroline-3-methyl)-methanthiosulfonate (Fig. 1, left) [13]. The modified side chain resulting from the reaction is often designated as R1. For a variety of reasons, side chain R1 has become the spin label of choice in SDSL studies. On one hand, R1 is tolerated surprisingly well at the vast majority of sites at which it has been introduced in many different proteins. On the other hand, its EPR spectra are exquisitely sensitive to features of the local environment and provide a fingerprint for virtually every site [14].

Other possible spin labels specific for sulfhydryl groups are nitroxides containing an iodoacetamide group [15]. Spin labels featuring different specificity are available [16, 17]. After the labeling procedure, excess spin label should be removed, for instance using a size exclusion spin column. For labeling procedures, see [148].

Nitroxide spin labels are small and have been shown to have minimal effects on protein structures [18, 19]. However, for SDSL, as for all labeling techniques, control experiments comparing wild type protein and labeled mutants are essential to exclude distortion of protein conformation and function due to the label.

An alternative strategy for the introduction of spin labels can be used in protein and peptide chemistry by spin label building blocks, e.g., 4-amino-1-oxyl-2,2,6,6-tetramethyl-piperidine-4-carboxylic acid (TOAC, Fig. 1, right) which are directly incorporated into the peptide during chemical synthesis [20–25].

2 SDSL EPR Methods

From EPR experiments with spin labels, four primary parameters are obtained: (1) side chain mobility, (2) distances to other paramagnetic centers, e.g., a second spin label or a metal ion within the very same or another molecule, (3) solvent

and oxygen accessibility, and (4) a measure for polarity of the environment of the spin-label.

In the following sections methods for obtaining the first three types of information are explained. Polarity measurements are particularly useful for membrane proteins and are reviewed in [148].

2.1 Mobility Measurements

The typical CW EPR spectrum of nitroxide labels in X band consists of three lines due to the hyperfine interaction with the ^{14}N nucleus featuring a nuclear spin $I = 1$. As a consequence of the common experimental procedure which includes signal detection using a lock-in technique, EPR spectra are usually shown as first derivatives of the absorption spectrum (Fig. 2). In a homogeneous magnetic field the EPR signal does not depend on the spatial position of the label, and therefore motion and translational diffusion cannot be detected unless applying magnetic field gradients [27, 28]. However, since the Zeeman interaction and, in particular, the hyperfine interaction of nitroxides are anisotropic, the EPR signal is sensitive to the molecular orientation of the label with respect to the external magnetic field. Thus, rotational diffusion can generally be detected by EPR.

Rotation of the label with correlation times of the order of the inverse width of the nitroxide spectrum (5.5 ns) partially averages the anisotropy, resulting in spectral changes (Fig. 2). Slight narrowing of the spectrum is detectable up to rotational correlation times of 1 μs and anisotropy-related line broadening is detectable down to rotational correlation times of 10 ps. Therefore, SDSL EPR is sensitive to dynamics on the picosecond to microsecond timescales, covering a variety of the important biological molecular mechanisms such as the dynamics of proteins in solution [29–31].

Fig. 2 Simulated EPR spectra for nitroxides in X band (9.7 GHz) assuming different (isotropic) rotational mobilities. (a) Very fast rotational mobility corresponding to the isotropic limit, rotational mobilities corresponding to rotational correlation times of (b) 100 ps, (c) 1 ns, (d) 3 ns, (e) 10 ns, (f) very slow rotational mobility corresponding to rigid limit. Simulated using EasySpin functions Garlic (a–c), Chili (d, e), and Pepper (f) [26]
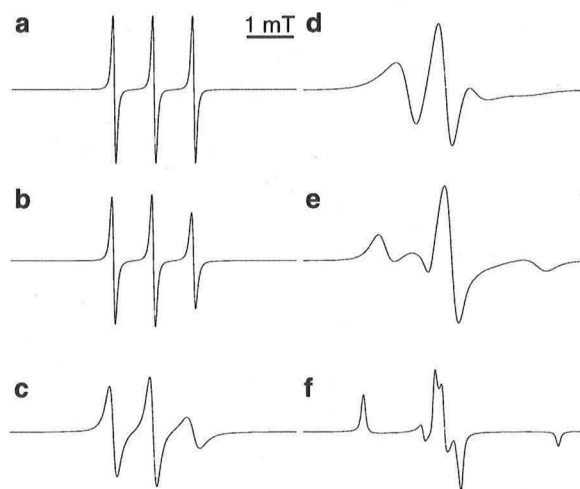
The spectra do not directly report on the dynamics of the labeled macromolecule as a whole but contain information on three types of motion: (1) internal motion of the nitroxide about the chemical bonds of the linker (cf. Fig. 1, left), (2) motion of the site of attachment relative to the rest of the macromolecule (conformational flexibility), and (3) motion of the macromolecule as a whole. The internal motion of the label may be restricted by the environment, depending on the extent to which the molecular environment engulfs the label. These three dynamic components significantly complicate the spectral analysis. However, a spectrum can often be approximated by a simple motional model to provide information on the properties of the macromolecule [32]. Temperature dependent experiments can adjust the contributions of the different types of motion to the motional properties reported by the EPR spectra [33].

The accessible timescale depends on the experimental frequency, e.g., the slow overall and collective motion will show up best at lower operating frequencies and fast motion will show up best at higher operating frequencies. In particular, high field EPR can be used to analyze anisotropic motional dynamics.

One EPR spectrum measured at one single frequency does not allow complete description of the spin label motion. Therefore, multifrequency EPR studies are preferable to separate various motional modes in a protein according to their timescales [34, 35].

In order to analyze the rotational mobility of the spin label quantitatively, spectral simulations are required. Simulation programs for CW EPR spectra are available [26, 36–38]. For the case of fast isotropic motion, approximate values of the rotational correlation time can be calculated from the line height ratios [39].

A semiquantitative measure for nitroxide mobility is the inverse central line width [18], another measure is the inverse second moment of the entire spectrum. Plotting the inverse central line width vs the inverse second moment allows for distinguishing different topological regions. So, different categories, namely sites in loops or unfolded regions, sites on the surface of ordered structures, e.g., helices, or sites that are buried inside the core of a protein can be identified [18, 40–43]. The periodic dependence of mobility along a sequence can be used to identify secondary structure elements and protein topography [44].

While quantitative labeling is often checked by mass spectrometry, free labels and labels attached to a macromolecule can be distinguished by EPR mobility measurements (Fig. 3). For comparison, the correlation time of the unbound, free label in aqueous solution at room temperature is ~0.05 ns; in the example shown in Fig. 3 its mobility is reduced to a correlation time of 0.8 ns upon attachment to a protein fragment. Labels immobilized in well folded proteins feature typical correlation times in the order of several nanoseconds [46].

2.2 Distance Measurements

Exploiting different experimental approaches, EPR spectroscopy can access distances between paramagnetic centers in the range between 1 and 8 nm [1, 13, 47–54].

Fig. 3 Experimental CW
EPR spectra of free label
(*black*) and the same label
attached to a soluble protein
fragment (TonB) in aqueous
solution at room temperature
in X band. (Experimental data
taken from [45])
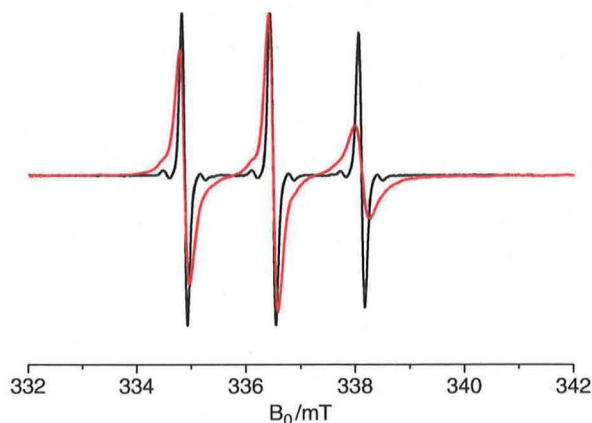
By proper data analysis, distance *distributions* can be obtained [55–61] allowing for
analyzing flexible structures or coexisting conformations. Such techniques have
been successfully applied on soluble proteins [62–64].

While the complementary technique Förster resonant energy transfer (FRET),
which is widely used for studying distances in proteins requires two different,
relatively large chromophores, which must be chosen according to the expected
distance, EPR distance measurements can be performed using two identical much
smaller nitroxide labels and are precise over a broad range of distances [51, 65, 66].

Depending on the labeling strategy, inter- and intramolecular distances are
accessible. While for measuring intramolecular distance constraints doubly spin
labeled molecules can be used, intermolecular distances can be determined between
singly labeled molecules (Fig. 4).

Distance measurements by EPR rely on the dipole–dipole coupling between
spins, which is inversely proportional to the cube of the distance [67]. Additionally,
the dipole–dipole coupling also depends on the angle between the spin–spin vector
and the magnetic field (Fig. 5a). For oriented samples this angular dependency can
be observed (Fig. 5b). Fast reorientation of the spin–spin vector, e.g., fast rotational
diffusion of the doubly labeled protein under investigation, results in averaging
over all possible orientations and cancels the dipole–dipole interaction to zero.
Therefore, most often distance measurements are performed in a frozen state upon
shock freezing in glass forming solution, e.g., aqueous buffer solution mixed with
glycerol, resulting in an isotropic orientation distribution. Hence, the dipolar spec-
trum of such a macroscopically isotropic sample consists of a superposition of
dipolar spectra of all possible orientations of the spin–spin-vector resulting in a
classic Pake pattern (Fig. 5c).

Folding kinetics of proteins can be determined by a combination of rapid freeze-
quench experiments and SDSL EPR distance measurement or stopped-flow EPR
[68, 69].

In EPR distance measurements, two cases have to be distinguished. For
distances between nitroxide spin labels below 2 nm the dipole–dipole coupling
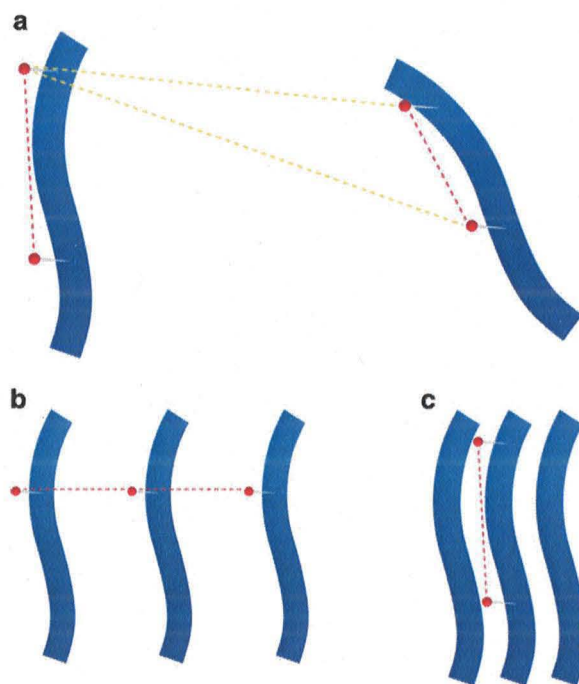
Fig. 4 Cartoon representation of EPR distance measurements. (**a**) Doubly labeled monomeric proteins give rise to intra- and intermolecular spin–spin interactions. In order to determine intramolecular distances, experimental data has to be corrected for intermolecular contributions. (**b**) Intermolecular distance measurements using singly labeled proteins in protein oligomers or aggregates. Multiples of the distance are also expected. This may be even more complicated for different types of aggregation and can be analyzed by studying a series of samples with increasing content of non-labeled molecules (diamagnetic dilution). (**c**) To measure intramolecular distances within oligomers/aggregates, a mixture of doubly labeled and non-labeled proteins can be used

exceeds the inhomogeneous line width of the EPR spectrum caused by unresolved hyperfine couplings and g-anisotropy. In this case, distances can be derived by CW EPR. For distances between nitroxide spin labels larger than approximately 2 nm, the dipole–dipole coupling is much smaller than competing interactions of the spin Hamiltonian. Thus the dipole–dipole coupling has to be separated from those larger interactions, which is usually done by pulsed EPR approaches, among these the four-pulse double electron electron resonance (DEER) [48, 51, 70, 71]. By using multiple techniques a more complete picture is obtained than can be found by a single technique [72]. In the borderline region of applicability of CW EPR and DEER (1.7–2.0 nm) both methods have to be combined in order to obtain accurate inter-nitroxide distances [73]. The lower limit of precise distance measurements is determined by the exchange coupling between two spins. With respect to the dipole–dipole interaction it can usually be neglected for distances larger than about 1.2 nm [74, 75]. On the other hand, for much shorter distances characteristic
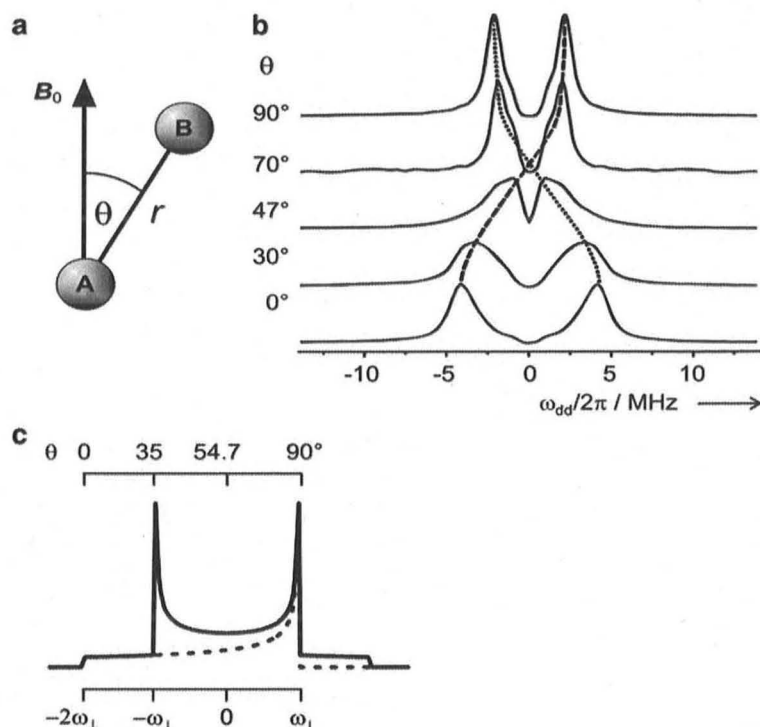
Fig. 5 (a) The dipole–dipole interaction between two spins A and B depends inter alia on the angle θ between the spin–spin-vector and the external magnetic field B_0. (b) This angular dependency can be observed for oriented samples as shown with this experimental data for a biradical in a liquid crystal under different orientations. (c) Simulated dipolar spectrum for a macroscopically isotropic sample (*Pake pattern*). Adapted from [66], copyright Wiley-VCH Verlag GmbH and Co. KGaA. Reproduced with permission

exchange narrowed single line EPR spectra indicate orbital overlap between multiple spin labels in close contact [76–78].

2.2.1 CW EPR Experiments

CW EPR experiments for distance determination can be performed on standard spectrometers, most commonly in X band which are quite generally accessible, and the measurements are technically not very demanding. Typical sample volumes are 50 μL at concentrations of about 50 μM.

Distances in solution at physiological temperatures can at least be estimated under conditions where the reorientation rate of the spin–spin-vector is reduced by other mechanisms, e.g., embedding the proteins in membranes or upon addition of viscosity agents [79]. In this case the dipole–dipole interaction is partly averaged out, making accurate distance measurement difficult. Quantitative

Fig. 6 Spin-normalized EPR spectra of aggregated peptides showing dipolar broadening at $T = 120$ K. The broadened spectrum originates from a sample containing 100% singly labeled peptides (*red*), while the reference sample (*black*) contains 90% unlabeled and 10% singly labeled peptides. This diamagnetic dilution suppresses dipolar broadening. (Experimental data taken from [80])
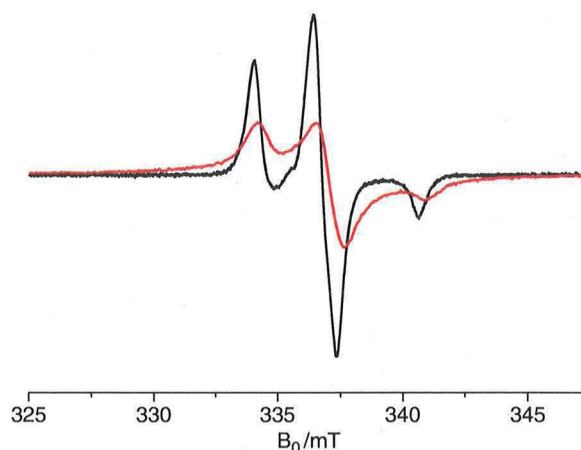
distance measurement is performed in frozen solution, the optimum temperature being $T = 120$ K.

Dipolar interaction can lead to an EPR line broadening (Fig. 6). The spectrum of the interacting spins can be treated as the convolution of the non-interacting powder pattern spectrum with a dipolar broadening function which is known as Pake pattern in randomly oriented samples.

When EPR spectra are normalized to the same number of contributing spins (as in Fig. 6), dipolar broadening is apparent by a decrease of the signal amplitude, which can be recognized more easily.

The non-interacting powder pattern which is required for distance analysis is experimentally accessible by measuring EPR spectra of samples containing either singly labeled proteins or, in the case of intermolecular distances, containing both labeled and unlabeled proteins ("diamagnetic dilution") to avoid interspin distances below 2.0 nm.

Software for extraction of distances from CW spectra, e.g., by analysis of spectral lineshapes by simulation or lineshape deconvolution [50, 81], is available and reviewed in [148].

2.2.2 Pulsed Methods

Pulsed methods [82] increase the range of distance sensitivity. They can be used to separate the dipole–dipole interaction from other contributions of the spin Hamiltonian. At very large available microwave power, distances can be measured well by double quantum coherence (DQC) that uses a single frequency. With the power available on commercial spectrometers, double electron electron resonance [DEER, an acronym which is synonymously used with PELDOR (Pulsed Electron Double Resonance)] is the more sensitive technique and is thus most widely applied in the
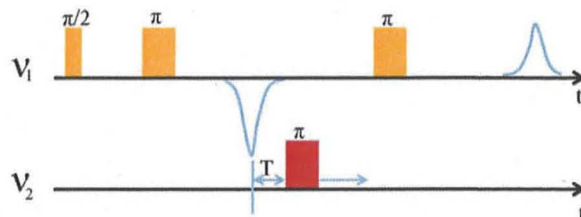
Fig. 7 Pulse sequence of the dead-time free four-pulse DEER experiment. The pulse sequence at frequency ν_1 (refocused spin echo) addresses the A spins, only, while the pulse at ν_2 flips the B spins. Applying the pump pulse at variable time T results in a modulation of the refocused echo intensity V (cf. Fig. 8a)

field. It requires a pulsed EPR spectrometer equipped with a two-frequency setup, which are commercially available. The DEER pulse sequence is depicted in Fig. 7 and is described below. Measurements are typically conducted using the dead-time free four-pulse DEER sequence and require typically 12 h of signal averaging for biological samples in X band [70]. Note in this context that one DEER measurement most often enables one to derive *one* distance constraint, only.

The Four-Pulse DEER Experiment

Originally, DEER was introduced as a three-pulse experiment [83, 84]. The dead time inherent with this pulse sequence prevents one from recording the important first data points of the DEER curve. Therefore, a dead-time free four-pulse variant of DEER was introduced [70] and is now used extensively.

The pulse sequence of the four-pulse DEER experiment is shown in Fig. 7. We consider a system of electron spins A (observer spins) and B (pumped spins) possessing a resonant microwave frequency ν_1 and ν_2, respectively. Spins A and B are usually chemically identical nitroxide labels. Since the nitroxide spectrum features a width of approximately 180 MHz, it is possible to apply pulses at two different frequencies with non-overlapping excitation profiles and subsequently divide the nitroxides in the sample into A- and B-spins, respectively. Accordingly, the pulse sequence at ν_1 addresses the A spins only, while the pulse at ν_2 flips the B spins. At frequency ν_1 a two-pulse Hahn-echo sequence is first applied resulting in an echo depicted in Fig. 7 with negative phase, which is followed by a third pulse at this so-called observer frequency which leads to a refocused echo of the observer spins A. The dipolar interaction can be studied by insertion of an additional π-pulse at the second frequency ν_2 between the two π-pulses at ν_1. This pulse affects the B spins only. Their inversion leads to a change of the local magnetic field at the A spins. Applying the pump pulse at variable time T results in a modulation of the refocused echo intensity V with the frequency of the dipolar coupling between A and B spins. Plotting V vs T yields the typical DEER curve (Fig. 8a).
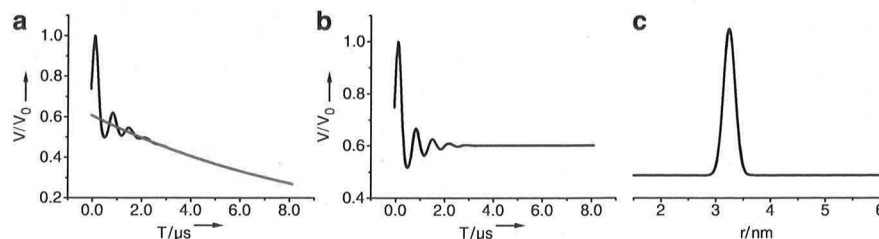
Fig. 8 (**a**) Simulated DEER data for a doubly labeled model system. The intensity V of the refocused observer echo (cf. Fig. 7) is plotted vs the delay T of the pump pulse (*black*). The DEER curve can be corrected for a background signal (*red*) originating from intermolecular interactions (cf. Fig. 4a). (**b**) Dipolar evolution (form factor) derived from DEER data in (**a**) by correcting for the intermolecular background. (**c**) Corresponding distance distribution. Simulations were performed using DEERAnalysis [61]

Measuring in frozen solution is desired in order to avoid the averaging out of the dipole–dipole interactions and, in particular, the strong decrease in transverse relaxation time T_2 that is induced even by moderate spin label dynamics. Additionally, the proper choice of temperature is important in pulsed EPR to optimize relaxation rates. $T = 50$ K is ideal for DEER at nitroxides in aqueous solution, so liquid helium cooling is advantageous [85].

A dramatic increase in sensitivity can be obtained by lengthening the transverse relaxation time by choosing the right solvent. At low temperatures the transverse relaxation time is significantly longer in a fully deuterated matrix than in a protonated one. Deuteration of the underlying protein, as well as the solvent, extends the transverse relaxation time to a considerable degree and gives enhanced sensitivity and an extended accessible distance range [86].

Typical sample volumes for X-band measurements are in the order of some 10 μL at minimum concentration of some 10 μM. There is an optimum concentration depending on the required maximum accessible distance. For distances of up to 2.5 nm, concentrations up to 4 mM can be used; for measuring distances up to 8 nm, the concentration should not exceed 0.35 mM [66].

While most experiments reported in the literature were performed in X band, Q band DEER gains increasing attention owing to its superior sensitivity revealing higher-quality distance data as well as significantly increased sample throughput [87, 88]. DEER in W band gives access to the relative orientation of spin labels due to orientation selection at high fields. More precisely, selective excitation by microwave pulses may unravel if the orientation of the spin–spin vector is correlated to the orientations of the molecular frame of the two nitroxides [89, 90]. However, due to conformational freedom of the labels, such correlation is often not very strong.

In most cases, EPR distance measurements are performed to determine a distance within a nanoobject, e.g., the spin–spin distance in a doubly labeled protein. It is desirable to consider an isolated pair of spin labels; therefore dipolar interactions to spins of neighboring objects, e.g., intermolecular interactions,

should be suppressed. This can be achieved by diamagnetic dilution, e.g., mixing with non-labeled wild type protein or protein labeled with a diamagnetic label analog. In the case of studying intramolecular distances in protein oligomers, diamagnetic dilution is of particular importance (cf. Fig. 8) [79, 91].

In any case, the DEER signal has to be corrected for the background originating from couplings to spins outside of the interesting nanoobject (Fig. 8a) [85]. Experimental background functions can be derived from singly labeled samples; they can be used for correcting the background in corresponding doubly labeled samples. If experimental background functions from singly labeled molecules are not available, theoretical functions taking homogeneous distributions of nanoobjects into account can be applied for correction. In many samples the distribution is homogeneous in $d = 3$ dimensions. Proteins bound to a membrane surface may be confined to $d = 2$ dimensions.

The data after background correction is often referred to as form factor (Fig. 8b).

The assumption of well separated spin pairs may not always be valid, e.g., in singly labeled trimers. Those cases lead to signal contributions from sum and difference combinations of dipolar frequencies which are not easy to analyze in terms of distances [92].

However, a parameter being rather easily determined is the number of spins per nanoobject, e.g., the number of proteins in an oligomer [57, 93, 94]. It is directly related to the modulation depth of the DEER curve after background correction, which additionally depends strongly on the excitation position, length, and flip angle of the pump pulse. Uncertainty in the degree of spin labeling affects interpretation of the oligomerization state [93–95]. In turn, reduced modulation depth for intramolecular distance measurements can indicate a fraction of de facto singly labeled molecules.

In analogy, from the background of the DEER signal reflecting homogeneously distributed spins, *local* spin concentrations up to 20 mM can be measured [96].

For evaluation of experimental DEER data several software packages are available [59, 61]. They cater either for data analysis based on a model of the distance distribution [97–99] or for model-free methods, e.g., Tikhonov regularization [57, 59]. For the model-free approach, the underlying mathematical problem is (moderately) ill-posed, i.e., quality of the analyzed data is very crucial. Incomplete labeling of double mutants results in (1) lower signal to noise of the primary data with increasing number of completely unlabelled molecules and (2) reduced modulation depth with decreasing number of doubly labeled molecules.

It is important to note that the distance between the spin density on the nitroxides differs from the corresponding distances of the protein backbone, since distance measurements utilize spin-labels as MTSSL which possess a number of single bonds in their linker allowing for different rotamers (Fig. 1 left) and thus are not conformationally unambiguous [100]. This introduces an uncertainty of the backbone–spin distance and complicates the interpretation of the spin–spin distances in terms of the protein backbone [64], although the uncertainty becomes less important for longer distances between the labeled sites [101].

This uncertainty can be reduced by molecular modeling of the spin label behavior. Several approaches were made to overcome this problem [64, 102, 103]. For instance, the program package MMM describes spin labels by a set of alternative conformations, rotamers, which can be attached without serious clashes with atoms of other residues or cofactors. The individual rotamers are assigned Boltzmann populations corresponding to an estimate of the sum of their internal energy and interaction energy with the protein. All simulations of experiments on spin labels are then based on the population weighted average over the ensemble of rotamers [104].

Experimental data for DEER experiments can be predicted for a modeled structure and favorable attachment sites can be predicted by scanning the whole protein [105].

2.3 Accessibility Measurements

Secondary structure can be obtained by studying the accessibility of the nitroxide label to paramagnetic colliders. The collision rate (more precisely the Heisenberg exchange frequency) with the spin label influences the relaxation time of the latter which can be measured and be used to estimate the local concentration of a paramagnetic quencher near a nitroxide spin label.

Water-soluble quenchers are transition metal complexes such as chelated nickel [nickel(II)-ethylenediamine-N,N'-diacetic acid (NiEDDA)]. A ubiquitous paramagnetic quencher is triplet oxygen, which is much more soluble in apolar environments, such as lipid bilayers, than in polar environments [3, 106]. As a consequence, by measuring the respective local concentration, membrane-exposed sites can be distinguished from solvent-exposed sites.

At very high local concentrations such quenchers cause line broadening. At low local concentration exchange broadening is insignificant and the transverse relaxation time T_2 is the same in the presence and absence of the quencher. In this case, the influence of the quenchers on the longitudinal relaxation time T_1 can be quantified by measuring saturation curves. For this, the peak-to-peak amplitude of the first derivative central line of the nitroxide spectrum is measured as a function of microwave power. Measuring on a reference substance such as dilute diphenylpicrylhydrazyl powder in KCl and defining a dimensionless accessibility parameter Π enables one to eliminate the dependency of those saturation curves on T_2 and the conversion efficiency of the microwave resonator [107–110].

3 Applications to Intrinsically Disordered Proteins

The most powerful techniques for protein structure determination in general are X-ray crystallography and nuclear magnetic resonance (NMR) spectroscopy. Very limited structural information is available if these techniques are not applicable.

This holds true for many membrane proteins which are difficult to crystallize or concentrate; therefore the determination of their structures is one of the most challenging fields in structural biology. Furthermore, structure determination of membrane proteins is an important application of SDSL EPR which is reviewed [33, 111–113, 148].

X-ray crystallography and NMR spectroscopy are also less successful in determination of structure and dynamics of IDPs [114]. IDPs have been recognized as a unique protein class as well, justified by the clear structural and functional separation which they have in common, and again, SDSL EPR can significantly contribute to their characterization as illustrated in the following.

IDPs comprise a large fraction of eukaryotic proteins (>30%). They lack a well-defined three-dimensional fold and display remarkable conformational flexibility. This property potentially enables them to be promiscuous in their interactions and to adapt their structure according to the needed function.

Since structure and dynamics of IDPs drastically depend on the environment, corresponding details are notoriously difficult to unravel. Because of their inherent flexibility, IDPs often fail to crystallize in their free form. When crystallization is successful, it only leads to a snapshot of a single conformation not representing the whole conformational ensemble [115]. The most common goal of structural studies, the determination of unique high-resolution structures, is not attainable for IDPs due to the absence of a well-defined structure.

Upon interaction with other cellular components, IDPs adopt more highly ordered conformations. These are subject to high-resolution structures in some cases; however, at least in some cases, the bound states of IDPs remain highly non-compact and retain substantial mobility [116, 117].

SDSL EPR offers a powerful tool to study IDPs. Nitroxide spin labels introduce a minimal perturbation of the system, and probe the very local environment of the label [3, 4, 38, 118]. The higher sensitivity of EPR compared to NMR allows for much lower concentrations of protein samples.

Several IDPs have already been subjected to SDSL EPR investigations. So EPR data showed decreased flexibility in a region of residual helical structure in the disordered C-terminal domain of the measles virus nucleoprotein, and demonstrated the further ordering of this region upon interaction with a binding partner [119, 120].

The amyloid β peptide Aβ was the subject of several studies [91, 121–123]; structural constraints on Aβ_{1-40} fibrils were obtained from measurements of CW EPR spectra and determination of spin–spin couplings in a series of spin-labeled cysteine mutant samples. Conclusions about molecular structure and supramolecular organization were drawn from these data. The observation of co-fibrillization of Aβ_{1-40} and Aβ_{1-42} suggested the absence of large structural differences between Aβ_{1-40} and Aβ_{1-42} fibrils.

Further examples of IDPs studied by SDSL EPR are the prion protein H1 [124], ubiquitin [125], or serum albumin [12]. In the following, recent results concerning α-synuclein are reviewed to illustrate the potential of SDSL EPR in the field of IDPs.

3.1 α-Synuclein

Intrinsic disorder is highly abundant among proteins associated with neurodegenerative diseases. The canonical model among the IDPs is α-synuclein (ASYN), a 140-residue protein that is abundantly present in the Lewy bodies characteristic of Parkinson's disease (PD). PD is the most common age-related movement disorder and the second most common neurodegenerative disorder. ASYN with its high propensity to aggregate and its conformational flexibility is an ideal model system for IDPs and for understanding PD and related disorders.

Depending on the environment, it adopts a variety of structurally distinct conformations including the intrinsically unfolded state, an amyloidogenic partially folded conformation, and different α-helical and β-sheet conformations. This conformational flexibility led to the term "protein-chameleon."

The exact physiological role of ASYN has yet to be determined, but membrane binding seems to be important for its function. As a consequence, the membrane bound form has received considerable attention in the last several years. Preferentially, ASYN binds to negatively charged lipid surfaces.

Human ASYN does not contain any cysteine residues. Singly and doubly labeled ASYN derivatives can be generated by site-directed mutagenesis introducing cysteines and subsequent spin labeling with MTSSL. Spin-labeled ASYN in solution at room temperature gives rise to sharp EPR line shapes characteristic for loop or unfolded regions indicating that ASYN is intrinsically disordered, e.g., largely unfolded in solution (Fig. 9a, b).

Fig. 9 CW EPR spectra at room temperature of (**a**) ASYN labeled at residue 140 in solution (*black*) and upon vesicle binding (*blue*), and ASYN labeled at residue 90 (**b**) in solution and (**c**) upon vesicle binding including corresponding spectral simulations (*red*). Taken from [126]
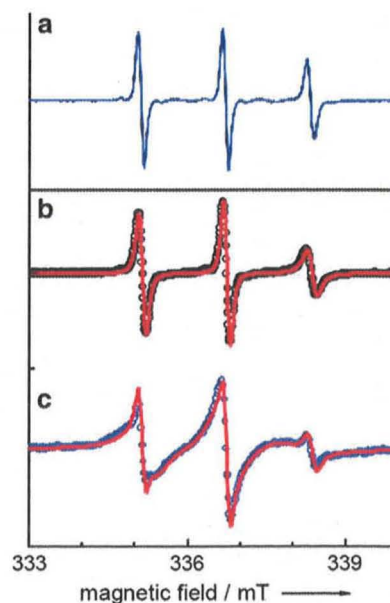
3.1.1 Fibrils

The aggregation of proteins into amyloid fibrils is associated with several neurode-generative diseases. It is believed that the aggregation of ASYN from monomers by intermediates into amyloid fibrils is the toxic disease-causative mechanism of PD.

A large set of singly labeled ASYN derivatives were used in order to investigate the structural features of ASYN fibrils. Fibrils grown from spin-labeled ASYN featured a fibril morphology being very similar to fibrils taken from wild type ASYN as verified by electron microscopy. Additionally, co-mixing of wild type and labeled ASYN indicated that both species are able to adopt similar structures within the fibril, confirming that the introduction of a spin label is tolerated remarkably well in amyloid fibrils [91].

Analyzing the intermolecular spin–spin interaction within the fibrils in terms of dipolar broadening depending on diamagnetic dilution, it was shown that similar sites from different molecules come into close proximity. While the accuracy of this analysis was not sufficient to distinguish fully whether parallelism occurred between strands or sheets (corresponding to distances of 4.7 or 10 Å) [127], a highly ordered and specifically folded central core region of about 70 amino acids was identified. The N-terminus is structurally more heterogeneous; the C-terminus consisting of 40 amino acids is completely unfolded [128].

The latter encouraged Chen et al. [127] to employ a C-terminal truncation mutant of ASYN containing residues 1–115. This allowed for optimizing spectral quality and minimizing components from non-fibrillized protein or other back-ground labeling possibly due to codon mistranslation [129]. Single-line, exchange narrowed EPR spectra were observed for the majority of all sites within the core region of ASYN fibrils. Such exchange narrowing requires the orbital overlap between multiple spin labels in close contact and therewith confirmed that the core region of ASYN fibrils is arranged in a parallel, in-register structure wherein similar residues from different molecules are stacked on top of each other. This core region extends from residue 36 to residue 98 and is tightly packed. Accessibility measurements suggested the location of potential β-sheet regions within the fibril. Furthermore, the data provide structural constraints for generating three-dimensional models.

3.1.2 Membrane Binding

Not only misfolding and fibril formation of ASYN but also membrane binding are of particular interest, especially for unraveling its physiological role. The N-terminus of ASYN contains 7 repeats, each of which is made up of 11 amino acids. Sequence analysis suggested that this part is likely to mediate lipid interactions [130, 131]. NMR studies are limited by the size of the complex under investigation. Hence, the structural information available concerns NMR studies of ASYN on micelles [132–135].

Micelles, however, differ in important aspects from biological membranes. Micelles have typical diameters of 5 nm and therefore may be too small to mimic organellic membranes. In order to understand the conformational changes that occur upon membrane binding of monomeric ASYN, SDSL EPR was performed with ASYN bound to phospholipid vesicles, e.g., small or large unilamellar vesicles (SUVs or LUVs, respectively).

To characterize the structural changes induced by membrane binding, the EPR spectra of 47 singly spin labeled ASYN derivatives were recorded in solution and upon binding to small unilamellar vesicles [42, 128].

As already mentioned, spin-labeled ASYN in solution gives rise to sharp EPR line shapes characteristic of intrinsic disorder (Fig. 9a, b). Upon membrane binding, spectral changes were observed for ASYN derivatives labeled within the repeats region (Fig. 9c). In contrast, little or no changes were detected for labels at positions within the last 40 amino acids, confirming that conformational changes upon membrane binding do not occur within the C-terminal portion (Fig. 9a).

The spectra upon membrane binding still contained residual sharp spectral components allocated to unbound ASYN. The spectra can be corrected for this component by subtraction of the spectrum of the free label. Analyzing the resulting spectra originating exclusively from membrane bound ASYN labeled within the repeat region exhibited line shapes indicating lipid- or solvent-exposed helix surface sites.

Additionally, O_2 and NiEDDA accessibilities (ΠO_2 and $\Pi NiEDDA$, respectively) were determined for the labels in the repeat regions. Nonpolar O_2 preferentially partitions into the membrane whereas the more polar NiEDDA preferentially partitions into the solvent. As a consequence, membrane-exposed sites show enhanced accessibility to O_2, whereas solvent-exposed sites are preferentially accessible to NiEDDA. In agreement with the formation of a helical structure, ΠO_2 and $\Pi NiEDDA$ exhibit continuous periodic oscillations. The accessibility data for both colliders can be conveniently summarized by the depth parameter Φ [$\Phi = \ln(\Pi O_2/\Pi NiEDDA)$] (Fig. 10), which increases linearly with increasing immersion depth [136].

The consecutive scan of the residues with respect to mobility and accessibilities demonstrates the formation of a single, elongated helix, wherein each 11 amino acid repeat takes up 3 helical turns.

Without subtracting the residual sharp spectral components of spin-labeled ASYN in the presence of SUVs, a multi-component spectral simulation strategy is required in order to describe the experimental data (Fig. 9b, c). Three different contributions featuring different isotropic rotational mobilities can be allocated to free spin labels, labeled residues not bound to SUVs, and residues bound to SUVs by the following approach. The spectra of ASYN in the absence of liposomes are well described by a superposition of two components, S_1 and S_2, where S_1 corresponds to the spectrum of the free spin label MTSSL measured independently. In the presence of SUVs, an additional component S_3 is needed, corresponding to the broadened part of the spectra. The shape of component S_3 and the prefactors
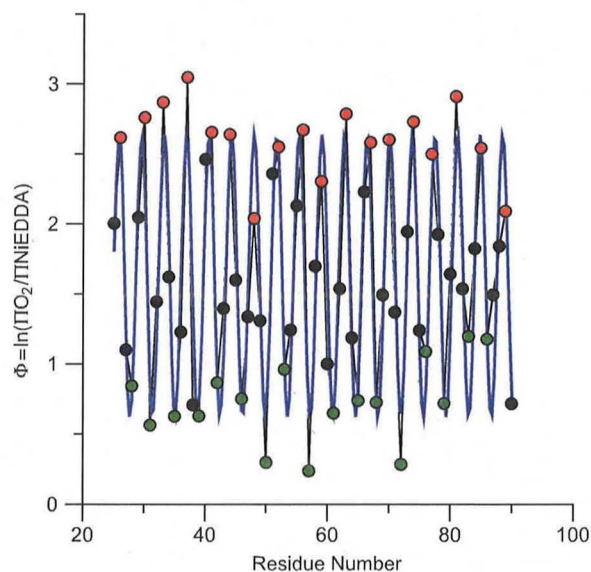
Fig. 10 Solvent accessibility analysis of singly labeled ASYN derivatives. The ratios of the accessibilities to O_2 and NiEDDA (ΠO_2 and Π NiEDDA, respectively) for residues 25–90 summarized by the depth parameter $\Phi = \ln(\Pi O_2/\Pi$ NiEDDA), with increasing Φ values indicating deeper membrane immersion depth. The *blue line* indicates the best fit to a cosine function and the resulting periodicity corresponds to the theoretically predicted periodicity of 3.67 amino acids per turn. Copyright 2005 National Academy of Sciences, USA, reproduced from [136]

a, b, and c are determined by least square fits to the data according to $S = aS_1 + bS_2 + cS_3$ [126].

Hence, the *local* binding affinity can be determined. Using this approach a systematic study varying the charge density of the membrane allowed for a locally resolved analysis of the protein–membrane binding affinity. The results showed that binding of ASYN to artificial phospholipid membranes is initiated by the N-terminus (Fig. 11) [126].

3.1.3 Conformation of Membrane Bound α-Synuclein

The NMR structure of ASYN bound to SDS micelles, commonly used for membrane mimicking, revealed a break in the helix, resulting in two antiparallel alpha-helices [132]. This model was confirmed by distance measurements exploiting SDSL EPR utilizing 13 different ASYN double mutants each containing 2 spin-labeled cysteines (horseshoe model, Fig. 12) [137].

In this study, one mutant includes a pair of cysteines placed within a single helix to provide an internal distance control. Distance distributions were obtained by DEER measurements and Tikhonov regularization. Studying ASYN bound to detergent and lysophospholipid micelles, it has been shown that the inter-helical
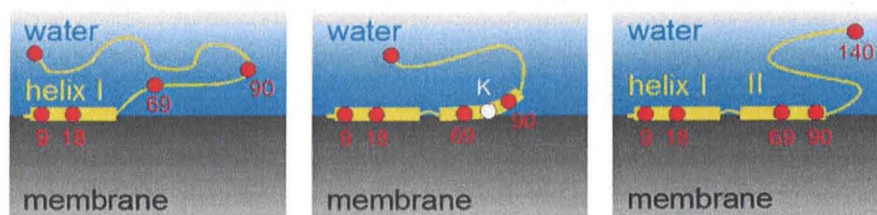
Fig. 11 Spin-label EPR revealed that ASYN membrane binding is triggered by its N-terminus. Schematic representation of ASYN at the membrane–water interface. Positions of spin labels used in this study are depicted as *red circles*, and the number of the labeled residue is given. Representing electrostatic interactions, the cationic residue K80 is shown as a *white circle*. Adapted from [126]

Fig. 12 Cartoon representation of the two helices and linker region of ASYN bound to an ellipsoidal micelle, illustrating the different distances measured using pulsed EPR (taken from [137])
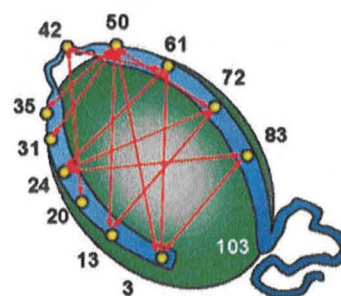
separation between the two helices formed upon binding to micelles is dependent on micelle composition, with micelles formed from longer acyl chains leading to an increased splaying of the two helices. The distance constraints were in accord with the NMR data. The data suggested that the topology of ASYN is not strongly constrained by the linker region between the two helices and instead depends on the geometry of the surface to which the protein is bound.

The geometry of micelles, however, differs significantly from those of biological membranes. Micelles have typical diameters of 5 nm and therefore may be too small to accommodate ASYN in the extended conformation (around 15 nm for an extended helix of 100 residues). Therefore, it had been postulated that the small size of the micelles may have artificially constrained the protein into a horseshoe structure.

A subsequent study considered two selected possible conformations for ASYN bound to SUVs, namely an extended helix and the horseshoe structure. Theoretically expected spin–spin distance distributions for doubly labeled ASYN taking the possible rotamers of the spin labels into account were calculated. This enabled one to identify label positions in the crucial location close to the potential linker region between the two horseshoe helices which would allow distinguishing between these conformations by CW EPR distance measurements. CW EPR spectra of correspondingly labeled ASYN bound to POPC SUVs were measured and, using the theoretical distance distributions, calculated. The authors interpreted their results in
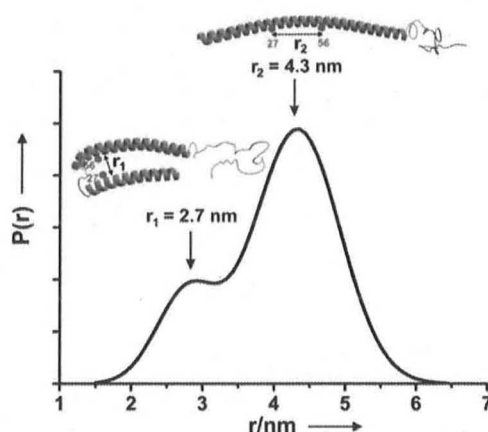
Fig. 13 The distance distribution for ASYN bound to LUV and labeled at residue 27 and 56 clearly consists of two contributions. The shorter distance agrees well with the expected distance of 2.7 nm for the horseshoe conformation derived from the NMR structure (pdb access code 1XQ8) while the longer distance is consistent with an extended alpha-helix. Taken from [140]

such a way that an unbroken helical structure around residue 40 was ruled out and confirmed the picture of the interhelix region characterized by conformational disorder [138]. Later, a close inspection of the data resulted in suggesting that the measured distances may be more consistent with an extended helix form than with the horseshoe model [139].

ASYN bound to vesicles, bicelles, and rodlike micelles was also studied by DEER allowing for measuring longer distances. Jao et al. reported results suggesting an extended helix conformation being significantly different from that of ASYN in the presence of SDS micelles. Their DEER study showed that for several double mutants the average distance per residue was ±1% of that for an alpha-helix, which argues strongly for an extended helix [137].

Already in this study, a number of samples have yielded somewhat bimodal distance distributions, suggesting distinct conformations of the protein. Actually, this was confirmed by a further DEER study [140], which used the ability of DEER to measure distance *distributions* for direct evidence of coexisting horseshoe and extended helix conformations of membrane bound ASYN (Fig. 13).

A DEER study [141] measuring distances of up to 8.7 nm showed that the PD-linked ASYN mutations also remain capable of adopting both structures, and that the protein to lipid ratio determines whether the protein adopts the broken or extended helix conformation.

This ability of ASYN to adopt different structures can provide an explanation of the disparate results obtained using similar experimental techniques and often with only slight variations in experimental conditions reported in the literature [99, 133–136, 138, 139, 142].

A complementary approach studying protein–membrane interaction by SDSL EPR is to utilize spin-labeled lipids. In the case of ASYN, different restrictions of

segmental motion in the chains of different lipids were observed upon ASYN binding. This observation indicates that ASYN associates at the interfacial region of the bilayer where it may favor a local concentration of certain phospholipids [143–146].

3.1.4 Lipid-Induced Aggregation

Using singly spin labeled mutants, *inter*molecular distances are also accessible by DEER. It was shown that ASYN may influence the membrane structure and even disrupt membranes. Under those conditions intra- and intermolecular distance measurements by DEER allowed for the conclusion that ASYN forms aggregates once in contact with SUVs [99, 147].

The simplest model for such an aggregate was proposed based on the distance constraints (Fig. 14). In these aggregates, two ASYN molecules are in close contact, but they could form part of a larger aggregate in which the proteins are arranged in an ordered fashion.

4 Concluding Remarks

SDSL EPR has developed as a powerful tool in order to study structure and dynamics of bio-macromolecules. Mobility and distance measurements being sensitive to dynamics on the picosecond to microsecond timescales, covering the
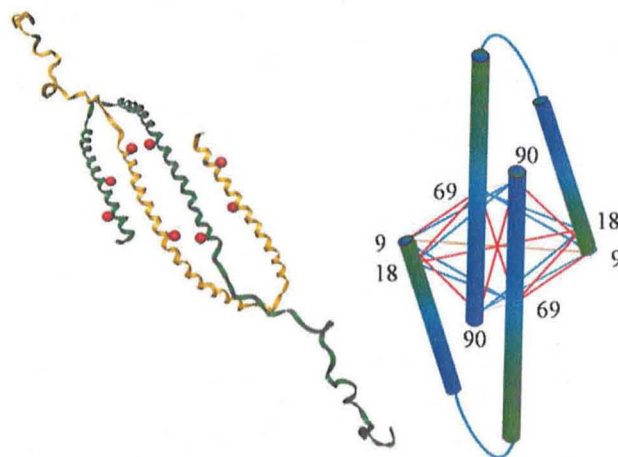

Fig. 14 *Left*: ASYN forms well-defined aggregates with lipids. In these aggregates, two ASYN molecules are in close contact, but they could form part of a larger aggregate in which the proteins are arranged in an ordered fashion. Spin labels are depicted as *red circles*. *Right*: Cartoon representation of EPR distance constraints. Taken from [141]

dynamics of proteins in solution, or giving access to distances between spin labels in the nanometer range, are probably amongst the most important experimental approaches.

Advantages of SDSL EPR include straightforward labeling procedures using one type of label for a broad accessible range in distance measurements, small size of label-molecules featuring minimal perturbations of the system under investigation, virtually no limitation of the size of the complex under study, and high sensitivity. Sophisticated pulsed EPR methods for distance determination compel by their unsurpassed accuracy as well as their ability to extract distance *distributions* and therefore to detect coexisting structures. Since unlabeled diamagnetic molecules are EPR silent, distance constraints can be obtained background free in (frozen) solution.

IDPs form a unique protein category characterized by the absence of a well-defined structure and by remarkable conformational flexibility. As a result of these properties, and because of its high potential, SDSL EPR is amongst the most suitable methods to study IDPs and will gain increasing attention in this rapidly advancing field. Recent results on α-synuclein show that SDSL EPR has now reached a level where broad application unraveling structure and dynamics of IDPs is feasible.

References

1. Hubbell WL, Altenbach C (1994) Investigation of structure and dynamics in membrane-proteins using site-directed spin-labeling. Curr Opin Struct Biol 4:566–573
2. Hubbell WL, McHaourab HS, Altenbach C, Lietzow MA (1996) Watching proteins move using site-directed spin labeling. Structure 4:779–783
3. Hubbell WL, Gross A, Langen R, Lietzow MA (1998) Recent advances in site-directed spin labeling of proteins. Curr Opin Struct Biol 8:649–656
4. Feix J, Klug C (1998) Site-directed spin labeling of membrane proteins and peptide-membrane interactions. In: Berliner LJ (ed) Biological magnetic resonance, vol 14. Plenum Press, New York
5. Likhtenshtein GI, Yamauchi J, Nakatsuji S, Smirnov AI, Tamura R (2008) Nitroxides. Wiley-VCH, Weinheim
6. Berliner LJ, Reuben J (1989) Spin labeling – theory and application. In: Biological magnetic resonance, vol 8. Academic, New York
7. Potapov A, Yagi H, Huber T, Jergic S, Dixon NE, Otting G, Goldfarb D (2010) Nanometer-scale distance measurements in proteins using Gd3+ spin labeling. J Am Chem Soc 132:9040–9048
8. Song Y, Meade TJ, Astashkin AV, Klein EL, Enemark JH, Raitsimring A (2011) Pulsed dipolar spectroscopy distance measurements in biomacromolecules labeled with Gd(III)

markers. J Magn Reson 210(1):59–68. doi:S1090-7807(11)00071-1 [pii] 10.1016/j.
jmr.2011.02.010

9. Axel FS (1976) Biophysics with nitroxyl radicals. Biophys Struct Mech 2:181–218

10. Klug CS, Feix JB (2008) Methods and applications of site-directed spin labeling EPR spectroscopy. In: Terry A (ed) Biophysical tools for biologists: vol one in vitro techniques, vol 84. Methods in Cell Biology. Academic, New York

11. Braun P, Nägele B, Wittmann V, Drescher M (2011) Mechanism of multivalent carbohy-drate-protein interactions studied by EPR spectroscopy. Angew Chem Int Ed, doi: 10.1002/anie.201104492

12. Junk MJN, Spiess HW, Hinderberger D (2010) The distribution of fatty acids reveals the functional structure of human serum albumin. Angew Chem Int Ed 49:8755–8759

13. Hubbell WL, Cafiso DS, Altenbach C (2000) Identifying conformational changes with site-directed spin labeling. Nat Struct Biol 7:735–739

14. Langen R, Oh KJ, Cascio D, Hubbell WL (2000) Crystal structures of spin labeled T4 lysozyme mutants: implications for the interpretation of EPR spectra in terms of structure. Biochemistry 39:8396–8405

15. Ogawa S, McConnel HM (1967) Spin-label study of hemoglobin conformations in solution. Proc Natl Acad Sci USA 58:19–26

16. Jahnke W, Rudisser S, Zurini M (2001) Spin label enhanced NMR screening. J Am Chem Soc 123:3149–3150

17. Lawrence JJ, Berne L, Ouvrierbuffet JL, Piette LH (1980) Spin-label study of histone H1-DNA interaction – comparative properties of the central part of the molecule and the N-amino and C-amino tails. Eur J Biochem 107:263–269

18. McHaourab HS, Lietzow MA, Hideg K, Hubbell WL (1996) Motion of spin-labeled side chains in T4 lysozyme, correlation with protein structure and dynamics. Biochemistry 35:7692–7704

19. Alexander RS, Nair SK, Christianson DW (1991) Engineering the hydrophobic pocket of carbonic anhydrase-II. Biochemistry 30:11064–11072

20. Becker CFW, Lausecker K, Balog M, Kalai T, Hideg K, Steinhoff HJ, Engelhard M (2005) Incorporation of spin-labelled amino acids into proteins. Magn Reson Chem 43:34–39

21. Karim CB, Zhang Z, Thomas DD (2007) Synthesis of TOAC spin-labeled proteins and reconstitution in lipid membranes. Nat Protoc 2:42–49

22. Toniolo C, Valente E, Formaggio F, Crisma M, Pilloni G, Corvaja C, Toffoletti A, Martinez GV, Hanson MP, Millhauser GL, George C, Flippen-Anderson JL (1995) Synthesis and conformational studies of peptides containing TOAC, a spin-labelled Cα, α-disubstituted glycine. J Pept Sci 1:45–57

23. Nakaie CR, Goissis G, Schreier S, Paiva ACM (1981) pH-Dependence of electron-paramag-netic-res spectra of nitroxides containing ionizable groups. Braz J Med Biol Res 14:173–180

24. Klare JP, Steinhoff HJ (2009) Spin labeling EPR. Photosynth Res 102:377–390

25. Bettio A, Gutewort V, Poppl A, Dinger MC, Zschornig O, Arnold K, Toniolo C, Beck-Sickinger AG (2002) Electron paramagnetic resonance backbone dynamics studies on spin-labelled neuropeptide Y analogues. J Pept Sci 8:671–682

26. Stoll S, Schweiger A (2006) EasySpin, a comprehensive software package for spectral simulation and analysis in EPR. J Magn Reson 178:42–55

27. Blank A, Talmon Y, Shklyar M, Shtirberg L, Harneit W (2008) Direct measurement of diffusion in liquid phase by electron spin resonance. Chem Phys Lett 465:147–152

28. Drescher M, Kaplan N, Dormann E (2006) Conduction-electron drift velocity measurement via electron spin resonance. Phys Rev Lett 96:037601

29. Dalton L (1985) EPR and advanced EPR studies of biological systems. CRC Press, Boca Raton

30. Berliner LJ, Reuben J (1998) Spin labeling – the next millenium. In: Biological magnetic resonace, vol 14. Academic, New York

31. Budil DE, Earle KA, Freed JH (1993) Full determination of the rotational diffusion tensor by electron-paramagnetic resonance at 250 GHz. J Phys Chem 97:1294–1303

32. Brustolon M (2008) What can be studied with electron paramagnetic resonance? In: Electron paramagnetic resonance. Wiley, Hoboken, New Jersey

33. Strancar J, Kavalenka A, Urbancic I, Ljubetic A, Hemminga MA (2010) SDSL-ESR-based protein structure characterization. Eur Biophys J Biophys Lett 39:499–511

34. Zhang ZW, Fleissner MR, Tipikin DS, Liang ZC, Moscicki JK, Earle KA, Hubbell WL, Freed JH (2010) Multifrequency electron spin resonance study of the dynamics of spin labeled T4 lysozyme. J Phys Chem B 114:5503–5521

35. Liang ZC, Freed JH (1999) An assessment of the applicability of multifrequency ESR to study the complex dynamics of biomolecules. J Phys Chem B 103:6384–6396

36. Hanson GR, Gates KE, Noble CJ, Griffin M, Mitchell A, Benson S (2004) XSophe-Sophe-XeprView (R). A computer simulation software suite (v. 1.1.3) for the analysis of continuous wave EPR spectra. J Inorg Biochem 98:903–916

37. Bax A (1989) Two-dimensional NMR and protein-structure. Annu Rev Biochem 58:223–256

38. Belle V, Fournel A, Woudstra M, Ranaldi S, Prieri F, Thome V, Currault J, Verger R, Guigliarelli B, Carriere F (2007) Probing the opening of the pancreatic lipase lid using site-directed spin labeling and EPR spectroscopy. Biochemistry 46:2205–2214

39. Lund J, Dalton H (1985) Further characterization of the FAD and FE2S2 redox centers of component-C, the NADH – acceptor reductase of the soluble methane monooxygenase of methylococcus-capsulatus (BATH). Europ J Biochem 147:291–296

40. Isas JM, Langen R, Haigler HT, Hubbell WL (2002) Structure and dynamics of a helical hairpin and loop region in annexin 12: a site-directed spin labeling study. Biochemistry 41:1464–1473

41. Margittai M, Fasshauer D, Pabst S, Jahn R, Langen R (2001) Homo- and heterooligomeric SNARE complexes studied by site-directed spin labeling. J Biol Chem 276:13169–13177

42. Jao CC, Der-Sarkissian A, Chen J, Langen R (2004) Structure of membrane-bound alpha-synuclein studied by site-directed spin labeling. Proc Natl Acad Sci USA 101:8331–8336

43. Alexander N, Bortolus M, Al-Mestarihi A, McHaourab H, Meilerl J (2008) De novo high-resolution protein structure determination from sparse spin-labeling EPR data. Structure 16:181–195

44. Gross A, Columbus L, Hideg K, Altenbach C, Hubbell WL (1999) Structure of the KcsA potassium channel from Streptomyces lividans: a site-directed spin labeling study of the second transmembrane segment. Biochemistry 38:10324–10335

45. Domingo Köhler S, Weber A, Howard SP, Welte W, Drescher M (2010) The proline-rich domain of TonB possesses an extended polyproline II-like conformation of sufficient length to span the periplasm of Gram-negative bacteria. Prot Sci 19:625–630

46. Steinhoff HJ (1990) Residual motion of hemoglobin-bound spin labels and protein dynamics – viscosity dependence of the rotational correlation times. Eur Biophys J 18:57–62

47. Constantine KL (2001) Evaluation of site-directed spin labeling for characterizing protein-ligand complexes using simulated restraints. Biophys J 81:1275–1284

48. Jeschke G, Polyhach Y (2007) Distance measurements on spin-labelled biomacromolecules by pulsed electron paramagnetic resonance. Phys Chem Chem Phys 9:1895–1910

49. Steinhoff HJ, Suess B (2003) Molecular mechanisms of gene regulation studied by site-directed spin labeling. Methods 29:188–195

50. Rabenstein MD, Shin YK (1995) Determination of the distance between 2 spin labels attached to a macromolecule. Proc Natl Acad Sci USA 92:8239–8243

51. Jeschke G, Bender A, Paulsen H, Zimmermann H, Godt A (2004) Sensitivity enhancement in pulse EPR distance measurements. J Magn Reson 169:1–12

52. Godt A, Schulte M, Zimmermann H, Jeschke G (2006) How flexible are poly(para-phenyleneethynylene)s? Angew Chem Int Ed 45:7560–7564

53. Borbat PP, Davis JH, Butcher SE, Freed JH (2004) Measurement of large distances in biomolecules using double-quantum filtered refocused electron spin-echoes. J Am Chem Soc 126:7746–7747

54. Berliner LJ, Eaton SS, Eaton GR (2002) Distance measurements in biological systems by EPR. In: Biological magnetic resonance, vol 19. Academic, New York

55. Jeschke G, Koch A, Jonas U, Godt A (2002) Direct conversion of EPR dipolar time evolution data to distance distributions. J Magn Reson 155:72–82

56. Bowman MK, Maryasov AG, Kim N, DeRose VJ (2004) Visualization of distance distribution from pulsed double electron-electron resonance data. Appl Magn Reson 26:23–39

57. Jeschke G, Panek G, Godt A, Bender A, Paulsen H (2004) Data analysis procedures for pulse ELDOR measurements of broad distance distributions. Appl Magn Reson 26:223–244

58. Milov AD, Tsvetkov YD, Formaggio F, Oancea S, Toniolo C, Raap J (2004) Solvent effect on the distance distribution between spin labels in aggregated spin labeled trichogin GA IV dimer peptides as studied by pulsed electron-electron double resonance. Phys Chem Chem Phys 6:3596–3603

59. Chiang YW, Borbat PP, Freed JH (2005) The determination of pair distance distributions by pulsed ESR using Tikhonov regularization. J Magn Reson 172:279–295

60. Chiang YW, Borbat PP, Freed JH (2005) Maximum entropy: a complement to Tikhonov regularization for determination of pair distance distributions by pulsed ESR. J Magn Reson 177:184–196

61. Jeschke G, Chechik V, Ionita P, Godt A, Zimmermann H, Banham J, Timmel CR, Hilger D, Jung H (2006) DeerAnalysis2006 – a comprehensive software package for analyzing pulsed ELDOR data. Appl Magn Reson 30:473–498

62. Zhou Z, DeSensi SC, Stein RA, Brandon S, Dixit M, McArdle EJ, Warren EM, Kroh HK, Song LK, Cobb CE, Hustedt EJ, Beth AH (2005) Solution structure of the cytoplasmic domain of erythrocyte membrane band 3 determined by site-directed spin labeling. Biochemistry 44:15115–15128

63. Nakamura M, Ueki S, Hara H, Arata T (2005) Calcium structural transition of human cardiac troponin C in reconstituted muscle fibres as studied by site-directed spin labelling. J Mol Biol 348:127–137

64. Fajer PG (2005) Site directed spin labelling and pulsed dipolar electron paramagnetic resonance (double electron-electron resonance) of force activation in muscle. J Phys Condens Mat 17:S1459–S1469

65. Jeschke G, Abbott RJM, Lea SM, Timmel CR, Banham JE (2006) The characterization of weak protein-protein interactions: evidence from DEER for the trimerization of a von Willebrand factor A domain in solution. Angew Chem Int Ed 45:1058–1061

66. Jeschke G (2002) Distance measurements in the nanometer range by pulse EPR. ChemPhysChem 3:927–932

67. Jeschke G, Spiess HW (2006) Distance measurements in solid-state NMR and EPR spectroscopy. In: Dolinšek J, Vilfan M, Žumer S (eds) Novel NMR and EPR techniques, vol 684. Lecture Notes in Physics, Springer, Berlin/Heidelberg

68. Dockter C, Volkov A, Bauer C, Polyhach Y, Joly-Lopez Z, Jeschke G, Paulsen H (2009) Refolding of the integral membrane protein light-harvesting complex II monitored by pulse EPR. Proc Natl Acad Sci USA 106:18485–18490

69. Qu KB, Vaughn JL, Sienkiewicz A, Scholes CP, Fetrow JS (1997) Kinetics and motional dynamics of spin-labeled yeast iso-1-cytochrome c.1. Stopped-flow electron paramagnetic resonance as a probe for protein folding/unfolding of the C-terminal helix spin-labeled at cysteine 102. Biochemistry 36:2884–2897

70. Pannier M, Veit S, Godt A, Jeschke G, Spiess HW (2000) Dead-time free measurement of dipole-dipole interactions between electron spins. J Magn Reson 142:331–340

71. Martin RE, Pannier M, Diederich F, Gramlich V, Hubrich M, Spiess HW (1998) Determination of end-to-end distances in a series of TEMPO diradicals of up to 2.8 nm length with a new four-pulse double electron electron resonance experiment. Angew Chem Int Ed 37:2834–2837

72. Persson M, Harbridge JR, Hammarstrom P, Mitri R, Martensson LG, Carlsson U, Eaton GR, Eaton SS (2001) Comparison of electron paramagnetic resonance methods to determine distances between spin labels on human carbonic anhydrase II. Biophys J 80:2886–2897

73. Banham JE, Baker CM, Ceola S, Day IJ, Grant GH, Groenen EJJ, Rodgers CT, Jeschke G, Timmel CR (2008) Distance measurements in the borderline region of applicability of CW EPR and DEER: a model study on a homologous series of spin-labelled peptides. J Magn Reson 191:202–218

74. Jeschke G (2002) Determination of the nanostructure of polymer materials by electron paramagnetic resonance spectroscopy. Macromol Rapid Commun 23(4):227–246

75. Riplinger C, Kao JPY, Rosen GM, Kathirvelu V, Eaton GR, Eaton SS, Kutateladze A, Neese F (2009) Interaction of radical pairs through-bond and through-space: scope and limitations of the point-dipole approximation in electron paramagnetic resonance spectroscopy. J Am Chem Soc 131(29):10092–10106

76. Margittai M, Langen R (2004) Template-assisted filament growth by parallel stacking of tau. Proc Natl Acad Sci USA 101:10278–10283

77. Margittai M, Langen R (2006) Side chain-dependent stacking modulates tau filament structure. J Biol Chem 281:37820–37827

78. Molin YN, Salikhov KM, Zamaraev KI (1980) Spin exchange. Springer, Berlin

79. Altenbach C, Oh KJ, Trabanino RJ, Hideg K, Hubbell WL (2001) Estimation of inter-residue distances in spin labeled proteins at physiological temperatures: experimental strategies and practical limitations. Biochemistry 40:15471–15482

80. Scarpelli F, Drescher M, Rutters-Meijneke T, Holt A, Rijkers DTS, Killian JA, Huber M (2009) Aggregation of transmembrane peptides studied by spin-label EPR. J Phys Chem B 113:12257–12264

81. Steinhoff HJ, Radzwill N, Thevis W, Lenz V, Brandenburg D, Antson A, Dodson G, Wollmer A (1997) Determination of interspin distances between spin labels attached to insulin: comparison of electron paramagnetic resonance data with the X-ray structure. Biophys J 73 (6):3287–3298

82. Schweiger A, Jeschke G (2005) Principles of pulse electron paramagnetic resonance. Oxford University Press, Oxford, reprinted 2005 edn

83. Milov AD, Ponomarev AB, Tsvetkov YD (1984) Electron electron double-resonance in electron-spin echo – model biradical systems and the sensitized photolysis of decalin. Chem Phys Lett 110(1):67–72

84. Milov AD, Salikohov KM, Shirov MD (1981) Application of endor in electron-spin echo for paramagnetic center space distribution in solids. Fiz Tverd Tela 23(4):975–982

85. Jeschke G (2011) DeerAnalysis2011 user manual. http://wwweprethzch/software/DeerAnalysis_2011_manual.pdf. Accessed 7 Apr 2011

86. Richard W, Bowman A, Sozudogru E, El-Mkami H, Owen-Hughes T, Norman DG (2010) EPR distance measurements in deuterated proteins. J Magn Reson 207:164–167

87. Zou P, Mchaourab HS (2010) Increased sensitivity and extended range of distance measurements in spin-labeled membrane proteins: Q-band double electron-electron resonance and nanoscale bilayers. Biophys J 98(6):L18–L20. doi:DOI 10.1016/j.bpj.2009.12.4193

88. Höfer P, Heilig R, Schmalbein D (2003) The superQ-FT accessory for pulsed EPR, ENDOR and ELDOR at 34 GHz. Bruker SpinReport 152(153):37–43

89. Larsen RG, Singel DJ (1993) Double electron-electron resonance spin-echo modulation – spectroscopic measurement of electron-spin pair separations in orientationally disordered solids. J Chem Phys 98:5134–5146

90. Lovett JE, Bowen AM, Timmel CR, Jones MW, Dilworth JR, Caprotti D, Bell SG, Wong LL, Harmer J (2009) Structural information from orientationally selective DEER spectroscopy. Phys Chem Chem Phys 11:6840–6848

91. Torok M, Milton S, Kayed R, Wu P, McIntire T, Glabe CG, Langen R (2002) Structural and dynamic features of Alzheimer's A beta peptide in amyloid fibrils studied by site-directed spin labeling. J Biol Chem 277:40810–40815

92. Jeschke G, Sajid M, Schulte M, Godt A (2009) Three-spin correlations in double electron-electron resonance. Phys Chem Chem Phys 11:6580–6591

93. Hilger D, Jung H, Padan E, Wegener C, Vogel KP, Steinhoff HJ, Jeschke G (2005) Assessing oligomerization of membrane proteins by four-pulse DEER: pH-dependent dimerization of NhaA Na+/H + antiporter of E-coli. Biophys J 89:1328–1338

94. Upadhyay AK, Borbat PP, Wang J, Freed JH, Edmondson DE (2008) Determination of the oligomeric states of human and rat monoamine oxidases in the outer mitochondrial membrane and octyl beta-D-glucopyranoside micelles using pulsed dipolar electron spin resonance spectroscopy. Biochemistry 47:1554–1566

95. Bode BE, Margraf D, Plackmeyer J, Durner G, Prisner TF, Schiemann O (2007) Counting the monomers in nanometer-sized oligomers by pulsed electron – electron double resonance. J Am Chem Soc 129:6736–6745

96. Jeschke G, Schlick S (2006) Spatial distribution of stabilizer-derived nitroxide radicals during thermal degradation of poly(acrylonitrile-butadiene-styrene) copolymers: a unified picture from pulsed ELDOR and ESR imaging. Phys Chem Chem Phys 8:4095–4103

97. Domingo Köhler S, Spitzbarth M, Diederichs K, Exner TE, Drescher M (2011) A short note on the analysis of distance measurements by electron paramagnetic resonance. J Magn Reson 208:167–170

98. Pannier M, Schops M, Schadler V, Wiesner U, Jeschke G, Spiess HW (2001) Characterization of ionic clusters in different ionically functionalized diblock copolymers by CW EPR and four-pulse double electron-electron resonance. Macromolecules 34:5555–5560

99. Drescher M, Veldhuis G, van Rooijen BD, Milikisyants S, Subramaniam V, Huber M (2008) Antiparallel arrangement of the helices of vesicle-bound alpha-synuclein. J Am Chem Soc 130:7796–7797

100. Sajid M, Jeschke G, Wiebcke M, Godt A (2009) Conformationally unambiguous spin labeling for distance measurements. Chemistry 15:12960–12962

101. Borbat PP, McHaourab HS, Freed JH (2002) Protein structure determination using long-distance constraints from double-quantum coherence ESR: study of T4 lysozyme. J Am Chem Soc 124:5304–5314

102. Sale K, Sar C, Sharp KA, Hideg K, Fajer PG (2002) Structural determination of spin label immobilization and orientation: a Monte Carlo minimization approach. J Magn Reson 156:104–112

103. Fajer P, Likai S, Liu YS, Perozo E, Budil D, Sale K (2004) Molecular modeling tools for dipolar EPR. Biophys J 86:191A

104. Polyhach Y, Bordignon E, Jeschke G (2011) Rotamer libraries of spin labelled cysteines for protein studies. Phys Chem Chem Phys 13(6):2356–2366. doi:Doi 10.1039/C0cp01865a

105. Polyhach Y, Jeschke G (2010) Prediction of favourable sites for spin labelling of proteins. Spectroscopy 24:651–659

106. Hubbell WL, Altenbach C, Hubbell CM, Khorana HG (2003) Rhodopsin structure, dynamics, and activation: a perspective from crystallography, site-directed spin labeling, sulfhydryl reactivity, and disulfide cross-linking. Adv Protein Chem 63:243–290

107. Altenbach C, Froncisz W, Hyde JS, Hubbell WL (1989) Conformation of spin-labeled melittin at membrane surfaces investigated by pulse saturation recovery and continuous wave power saturation electron-paramagnetic resonance. Biophys J 56:1183–1191

108. Altenbach C, Flitsch SL, Khorana HG, Hubbell WL (1989) Structural studies on transmembrane proteins 2 spin labeling of bacteriorhodopsin mutants at unique cysteines. Biochemistry 28:7806–7812

109. Percival PW, Hyde JS (1975) Pulsed EPR spectrometer 2. Rev Sci Instrum 46:1522–1529

110. Yin JJ, Pasenkiewiczgierula M, Hyde JS (1987) Lateral diffusion of lipids in membranes by pulse saturation recovery electron-spin-resonance. Proc Natl Acad Sci USA 84:964–968

111. Lacapere JJ, Pebay-Peyroula E, Neumann JM, Etchebest C (2007) Determining membrane protein structures: still a challenge! Trends Biochem Sci 32:259–270

112. Torres J, Stevens TJ, Samso M (2003) Membrane proteins: the 'Wild West' of structural biology. Trends Biochem Sci 28:174

113. Torres J, Stevens TJ, Samso M (2003) Membrane proteins: the 'Wild West' of structural biology. Trends Biochem Sci 28:137–144

114. Tompa P (2002) Intrinsically unstructured proteins. Trends Biochem Sci 27:527–533

115. Timsit Y, Allemand F, Chiaruttini C, Springer M (2006) Coexistence of two protein folding states in the crystal structure of ribosomal protein L20. EMBO Rep 7:1013–1018

116. Eliezer D (2009) Biophysical characterization of intrinsically disordered proteins. Curr Opin Struct Biol 19:23–30

117. Dyson HJ, Wright PE (2002) Coupling of folding and binding for unstructured proteins. Curr Opin Struct Biol 12:54–60

118. Biswas R, Kühne H, Brudvig GW, Gopalan V (2001) Use of EPR spectroscopy to study macromulecular structure and function. Sci Prog 84:45–68

119. Morin B, Bourhis JM, Belle V, Woudstra M, Carriere F, Guigliarelli B, Fournel A, Longhi S (2006) Assessing induced folding of an intrinsically disordered protein by site-directed spin-labeling electron paramagnetic resonance spectroscopy. J Phys Chem B 110:20596–20608

120. Belle V, Rouger S, Costanzo S, Liquiere E, Strancar J, Guigliarelli B, Fournel A, Longhi S (2008) Mapping alpha-helical induced folding within the intrinsically disordered C-terminal domain of the measles virus nucleoprotein by site-directed spin-labeling EPR spectroscopy. Proteins 73:973–988

121. Murakami K, Hara H, Masuda Y, Ohigashi H, Irie K (2007) Distance measurement between Tyr10 and Met35 in amyloid beta by site-directed spin-labeling ESR spectroscopy: implications for the stronger neurotoxicity of A beta 42 than A beta 40. Chembiochem 8:2308–2314

122. Iurascu MI, Cozma C, Tomczyk N, Rontree J, Desor M, Drescher M, Przybylski M (2009) Structural characterization of β-amyloid oligomer-aggregates by ion mobility mass spectrometry and electron spin resonance spectroscopy. Anal Bioanal Chem 395:2509–2519

123. Sepkhanova I, Drescher M, Meeuwenoord NJ, Limpens R, Koning RI, Filippov DV, Huber M (2009) Monitoring Alzheimer amyloid peptide aggregation by EPR. Appl Magn Reson 36:209–222

124. Lundberg KM, Stenland CJ, Cohen FE, Prusiner SB, Millhauser GL (1997) Kinetics and mechanism of amyloid formation by the prion protein H1 peptide as determined by time-dependent ESR. Chem Biol 4:345–355

125. Igarashi R, Sakai T, Hara H, Tenno T, Tanaka T, Tochio H, Shirakawa M (2010) Distance determination in proteins inside Xenopus laevis oocytes by double electron-electron resonance experiments. J Am Chem Soc 132:8228–8229

126. Drescher M, Godschalk F, Veldhuis G, van Rooijen BD, Subramaniam V, Huber M (2008) Spin-label EPR on alpha-synuclein reveals differences in the membrane binding affinity of the two antiparallel helices. Chembiochem 9:2411–2416

127. Chen M, Margittai M, Chen J, Langen R (2007) Investigation of alpha-synuclein fibril structure by site-directed spin labeling. J Biol Chem 282:24970–24979

128. Der-Sarkissian A, Jao CC, Chen J, Langen R (2003) Structural organization of alpha-synuclein fibrils studied by site-directed spin labeling. J Biol Chem 278:37530–37535

129. Masuda M, Dohmae N, Nonaka T, Oikawa T, Hisanaga SI, Goedert M, Hasegawa M (2006) Cysteine misincorporation in bacterially expressed human alpha-synuclein. FEBS Lett 580:1775–1779

130. George JM, Jin H, Woods WS, Clayton DF (1995) Characterization of a novel protein regulated during the critical period for song learning in the zebra finch. Neuron 15:361–372

131. Davidson WS, Jonas A, Clayton DF, George JM (1998) Stabilization of alpha-synuclein secondary structure upon binding to synthetic membranes. J Biol Chem 273:9443–9449

132. Ulmer TS, Bax A, Cole NB, Nussbaum RL (2005) Structure and dynamics of micelle-bound human alpha-synuclein. J Biol Chem 280:9595–9603

133. Chandra S, Chen XC, Rizo J, Jahn R, Sudhof TC (2003) A broken alpha-helix in folded alpha-synuclein. J Biol Chem 278:15313–15318

134. Bussell R, Eliezer D (2003) A structural and functional role for 11-mer repeats in alpha-synuclein and other exchangeable lipid binding proteins. J Mol Biol 329:763–778

135. Bussell R, Ramlall TF, Eliezer D (2005) Helix periodicity, topology, and dynamics of membrane-associated alpha-synuclein. Prot Sci 14:862–872

136. Jao CC, Hegde BG, Chen J, Haworth IS, Langen R (2008) Structure of membrane-bound alpha-synuclein from site-directed spin labeling and computational refinement. Proc Natl Acad Sci USA 105:19666–19671

137. Borbat P, Ramlall TF, Freed JH, Eliezer D (2006) Inter-helix distances in lysophospholipid micelle-bound alpha-synuclein from pulsed ESR measurements. J Am Chem Soc 128:10004–10005

138. Bortolus M, Tombolato F, Tessari I, Bisaglia M, Mammi S, Bubacco L, Ferrarini A, Maniero AL (2008) Broken helix in vesicle and micelle-bound alpha-synuclein: insights from site-directed spin labeling-EPR experiments and MD simulations. J Am Chem Soc 130:6690–6691

139. Georgieva ER, Ramlall TF, Borbat PP, Freed JH, Eliezer D (2008) Membrane-bound alpha-synuclein forms an extended helix: long-distance pulsed ESR measurements using vesicles, bicelles, and rodlike micelles. J Am Chem Soc 130:12856–12857

140. Robotta M, Braun P, van Rooijen B, Subramaniam V, Huber M, Drescher M (2011) Direct evidence of coexisting horseshoe and extended helix conformations of membrane-bound alpha-synuclein. Chemphyschem 12:267–269

141. Georgieva ER, Ramlall TF, Borbat PP, Freed JH, Eliezer D (2010) The lipid-binding domain of wild type and mutant alpha-synuclein compactness and interconversation between the broken and extended helix forms. J Biol Chem 285:28261–28274

142. Trexler AJ, Rhoades E (2009) Alpha-synuclein binds large unilamellar vesicles as an extended helix. Biochemistry 48:2304–2306

143. Ramakrishnan M, Jensen PH, Marsh D (2003) Alpha-synuclein association with phosphatidylglycerol probed by lipid spin labels. Biochemistry 42:12919–12926

144. Bussell R, Ramlall TF, Eliezer D (2005) Helix periodicity, topology, and dynamics of membrane-associated alpha-synuclein. Protein Sci 14(4):862–872. doi:Doi 10.1110/Ps.041255905

145. Kamp F, Beyer K (2006) Binding of alpha-synuclein affects the lipid packing in bilayers of small vesicles. J Biol Chem 281(14):9251–9259. doi:DOI 10.1074/jbc.M512292200

146. Ramakrishnan M, Jensen PH, Marsh D (2006) Association of alpha-synuclein and mutants with lipid membranes: spin-label ESR and polarized IR. Biochemistry 45(10):3386–3395. doi:10.1021/bi052344d

147. Drescher M, van Rooijen BD, Veldhuis G, Subramaniam V, Huber M (2010) A stable lipid-induced aggregate of alpha-synuclein. J Am Chem Soc 132:4080–4081

148. Bordignon E (2011) Site-directed spin labeling of membrane proteins. Top Curr Chem. doi:10.1007/128_2011_243